

Electric-field effects on a droplet microemulsion

M. E. Edwards* and X. L. Wu

Department of Physics and Astronomy, University of Pittsburgh, Pittsburgh, Pennsylvania 15260

J.-S. Wu

Department of Natural Sciences, Fayetteville State University, Fayetteville, North Carolina 28301

J. S. Huang

Exxon Research and Engineering Company, Route 22 East, Annandale, New Jersey 08801

H. Kellay

CPMOH, Universite Bordeaux I, 351 Cours de la Liberation, 33405 Talence Cedex, France

(Received 5 August 1997; revised manuscript received 15 September 1997)

The Kerr effect in a model three-component microemulsion has been investigated using an improved experimental setup. These new measurements, which cover a wide range of droplet volume fractions, $0% < \phi < 30%$, suggest that the Kerr coefficient K scales as ϕ^2 throughout the entire range of concentrations. This scaling behavior suggests that Kerr effect in the microemulsion is intrinsically a many-body problem rather than a single-body problem as previously suggested. It remains an intriguing possibility that the microemulsion forms clusters comprising many droplets even in dilute concentrations. [S1063-651X(98)01801-7]

PACS number(s): 82.70.Kj, 78.20.Fm, 36.40.-c

I. INTRODUCTION

Effects of an electric field on complex fluids have been investigated for a long time. One might therefore expect that most fundamental issues have been resolved. This is clearly not the case even for systems that have been extensively studied. Examples include effects of an electric field on a binary liquid mixture near its consolute point [1], and the unusual Kerr effects observed for droplet microemulsions [2]. In both cases controversies abound and have been lingering for many years. It appears that difficulties in understanding these systems are due to the presence of long-range, anisotropic density correlations resulting from a dipolar interaction [3]. In the case of a microemulsion, interfacial structures due to surfactant monolayers may have to be taken into account as well. In this paper we illustrate, through our extensive Kerr electro-optical measurements, that current theory, either based on a single droplet or a pair of droplets (dimer) description, is inadequate to explain our experimental results. We conclude, therefore, that a relevant theory will have to incorporate many-particle correlations in the presence of an electric field.

The system under investigation is a three-component microemulsion made of AOT surfactant (sodium di-2-ethylhexyl sulfosuccinate), an aliphatic oil, and water. This is a well-studied system with its structure and thermodynamic phases carefully characterized [4]. In particular, in dilute solutions water droplets are encapsulated by a monolayer of AOT molecules and dispersed in the oil continuum. The size of these droplets is determined by the amount of water present in the solution, and is typically in the range of 20–

100 Å in diameter. A peculiar feature of this microemulsion is observed when it is exposed to an electric field \vec{E} . For a wide range of droplet concentrations, the measured Kerr coefficient $K[\equiv(n_{\parallel} - n_{\perp})/E^2]$ is positive for large droplets, while it becomes negative as the droplet size is reduced below a certain critical value. Here n_{\parallel} and n_{\perp} are indices of refraction parallel and perpendicular to \vec{E} . Moreover, K in both the positive and the negative regimes scales as the square of the droplet concentration, $K \propto \phi^2$, for $0 < \phi < 30%$. It is noted that for $\phi < 1%$ the microemulsion may not be stable against phase separation [5], and the Kerr effect is essentially due to the oil phase. There are sufficient reasons to believe that the above behavior is rather universal, as the phenomenon has been observed for microemulsions made of different oils and different surfactants [6]. This universal behavior is encouraging in the sense that the effect is not due to specifics of the molecules used, but rather is caused by a common physical mechanism, which we seek to clarify in this experiment.

One of the early attempts to understand the sign change in K is based on a single-droplet model [7,8]. According to this model, the shape of a microemulsion droplet elongates along \vec{E} , giving rise to a positive contribution to K . However, the droplet shape deformation causes reorientation of surfactant molecules on the oil-water interface. This has a negative contribution to K , since in this case more surfactants are aligned perpendicular to the \vec{E} field than parallel to it. As shown in Ref. [7], K is dominated by the shape deformation for large droplets; whereas it is dominated by the surfactant reorientation for small droplets. Despite its partial success, the single-droplet model is inconsistent with the conspicuous ϕ^2 dependence as seen in a number of experiments [2,9].

The first theoretical calculation which can be reconciled with the sign change as well as the ϕ^2 dependence is the

*Present address: Department of Physics, Spelman College, Atlanta, GA 30314.

work of Mayer [10]. In this model Mayer assumed that droplets form pairs or dimers, and that an electron charge can move freely along the circle where the two droplets merge. Since the charge is located off the symmetric axis of the dimer, it gives rise to a permanent dipole moment. In the presence of an E field, the orientation of the dimer now depends on two competing effects: (i) the interaction between the permanent dipole moment and the \vec{E} field, and (ii) the interaction between the induced dipole moments and the \vec{E} field. The former tends to orient the dimer perpendicular to \vec{E} with a torque $\tau \propto R^2$; whereas the latter tends to orient the dimer parallel to \vec{E} with $\tau \propto R^3$. Hence K switches signs as the radius R of the droplets increases. Mayer's model makes a number of predictions that can be readily checked by experiments. For instance, it predicts that (1) the crossover radius R_C is nearly independent of the dielectric constant of the oil continuum, and (2) the value of R_C is ~ 40 Å, which is only a function of temperature. Moreover, in order for Mayer's model to be valid it also requires that the total number of dimers in the solution must be much smaller than that of the monomers, which can be easily calculated using the law of mass conservation.

To check the validity of these theoretical models and their limitations provides a strong motivation for the experiment reported here. The paper is organized as follows: In Sec. II the sample preparations and experimental setup are described. The measurement procedures are also described in the same section. In Sec. III our recent experimental results, including Kerr coefficients with different aliphatic oils, will be presented. A comparison of these measurements with theory will be presented in Sec. IV. Finally, in Sec. V a brief summary is given.

II. EXPERIMENT

A. Sample preparation

The microemulsion used was a mixture of three components: AOT (sodium di-2-ethylhexyl sulfosuccinate), an aliphatic oil, and water. While most of our experiments were carried out using decane, a set of measurements were performed using other members of the alkane series, allowing the dielectric constant of the oil continuum to be varied systematically without significantly changing the chemistry of the samples. Altogether the following oils were used in the experiment: hexane, octane, nonane, decane, and dodecane. For convenience the relevant physical parameters for the chemicals involved are listed in Table I. All of the chemicals were purchased from Aldrich Chemical Company and were used without further purification. Double-distilled and deionized water was used, which has a resistivity of $18.2 \times 10^6 \Omega \text{ cm}$.

For a ternary mixture, one needs two independent control parameters in order to specify its composition uniquely. In our experiment we chose (i) the droplet (disperse-phase) concentration

$$\phi \equiv (M_{\text{AOT}} + M_{\text{H}_2\text{O}}) / (M_{\text{AOT}} + M_{\text{H}_2\text{O}} + M_{\text{OIL}}),$$

and (ii) the molar ratio between the water and the surfactant,

TABLE I. Physical parameters for the oils, water, and AOT surfactant.

Name	M (g/mol)	ρ (g/cm ³)	$\epsilon(0)$	n
C ₆ H ₁₄ (hexane)	86	0.660	1.890	1.375
C ₈ H ₁₈ (octane)	114	0.702	1.948	1.397
C ₉ H ₂₀ (nonane)	128	0.718	1.972	1.405
C ₁₀ H ₂₂ (decane)	142	0.730	1.991	1.410
C ₁₂ H ₂₆ (dodecane)	170	0.749	2.015	1.422
H ₂ O (water)	18	0.997	78	1.333
AOT (surfactant)	445	1.305		1.468

$$\omega \equiv \frac{(\text{number of H}_2\text{O molecules})}{(\text{number of AOT molecules})} = \frac{M_{\text{H}_2\text{O}} W_{\text{AOT}}}{M_{\text{AOT}} W_{\text{H}_2\text{O}}},$$

where M_i and W_i are the mass and the molecular weight of species i . Measurements were carried out using a set of concentrations, $\phi = 1\%$, 1.5% , 2% , 2.5% , 3% , 3.25% , 3.5% , 3.8% , 4% , 4.5% , 5% , 7.5% , 10% , 15% , 20% , 25% , and 30% . For each concentration, more than twenty samples were made with ω varying from 0 to 36, corresponding to R roughly up to 100 Å. This set of measurements allows the ω dependence to be found for different ϕ . To accurately determine the ϕ dependence, independent measurements were also carried out with two samples having fixed ω values, 10 and 32, and a starting a concentration of $\phi = 20\%$. The samples were continuously diluted until ϕ approached zero. The prepared samples were well mixed using magnetic stirring bars, and by hand shaking. Assuming that all the surfactant molecules stay on the water-oil interface, and the solubility of water in oil is negligible, ω measures the volume-to-surface ratio of the dispersed phase. For a spherical microemulsion, such as ours, ω is therefore proportional to the average radius R of the droplets.

B. Apparatus

Figure 1 shows the experimental setup [11]. The optical train consists of a HeNe laser ($\lambda = 6328$ Å), a linear polarizer,

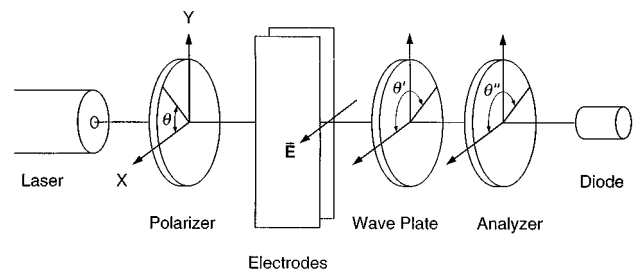


FIG. 1. Experimental setup. Our setup consists of a HeNe laser, a polarizer, a pair of electrodes, a quarter-wave plate, an analyzer, and a photodiode detector. The transmitted light couples to the photodiode detector through a multimode fiber optical cable, which is not shown in the figure. The applied electric field \vec{E} is in the horizontal \hat{X} direction. The optical axes of the polarizer, the quarter-wave plate, and the analyzer are set, respectively, at $\theta = \pi/4$, $\theta' = 3\pi/4$, and $\theta'' = 3\pi/4 - \alpha$.

izer, a sample cell, a quarter-wave plate, an analyzer, and a fast photodiode detector. The laser beam is weakly focused, and its polarization is 45° with respect to the applied \vec{E} field direction, which is set to the horizontal. The optical axis of the quarter-wave plate is 90° with respect to the polarizer while the optical axis of the analyzer is set at $90^\circ - \alpha$ with respect to the polarizer, as shown in Fig. 1. The use of the quarter-wave plate allows the positive and the negative birefringence to be differentiated, and at the same time increases the sensitivity of our apparatus. It can be shown [12,13] that, with the above setup, the transmitted light intensity at the detector is given by

$$I = I_0 \sin^2[\pi \Delta n L / \lambda + \alpha],$$

where I_0 is the incident light intensity, L is the path length of the sample cell, and $\Delta n (\equiv n_{\parallel} - n_{\perp})$ is the optical anisotropy. Note that for $\pi \Delta n L / \lambda \ll \alpha \ll 1$, I is proportional to Δn rather than Δn^2 , which would be the case in the absence of the quarter-wave plate. The transmitted intensity, in this case, can be written as

$$I \approx I_0 (\alpha^2 + 2\pi \Delta n \alpha L / \lambda).$$

Prior to a measurement, I_0 was calibrated independently for each solution with $\vec{E} = 0$ ($\Delta n = 0$). The transmission intensity I was measured as a function of α , and I_0 was then determined by fitting to the calibration curve using the quadratic equation $I = I_0 \alpha^2$. Once I_0 was found, a small but fixed retardation, typically in the range of $1^\circ < \alpha < 6^\circ$, was introduced into the optical path.

Our sample cell is made of quartz and has a path length $L = 10$ cm, which is ten times longer than our previous setup [2]. The large L is needed in order to determine the Kerr coefficients at low droplet concentrations accurately. The sample cell was carefully annealed so that strain birefringence on the windows was negligible. We can reliably measure optical phase shifts of the order of 10^{-4} , corresponding to $\Delta n \approx 10^{-8}$ or less.

The electrodes are made of two stainless-steel plates separated by two Teflon spacers. The distance between the electrodes is $d = 0.16$ cm, and is much smaller than the width ($W = 4$ cm) as well as the length ($L = 10$ cm) of the plates. The electric field between the electrodes, therefore, can be considered uniform. We used a Velonex high-voltage power supply to generate square pulses. The pulse height ($0 < V < 5000$ V) and pulse width ($10^{-6} < \Delta t < 3 \times 10^{-2}$ s) can be easily adjusted.

C. Measurement procedure

To calibrate our system, we used nitrobenzene, since its Kerr coefficient $K = 2.85 \times 10^{-18} \text{ m}^2/\text{V}^2$ is well known at the HeNe wavelength. The calibration procedure ensured that the measured K is accurate to less than 10%. Two competing effects come into play in the electric birefringence measurements. On the one hand, one would like to achieve a better signal-to-noise ratio, which requires a long measurement time; on the other hand, one would also like to minimize the Joule heating due to a conduction current, which requires a short measurement time. For small droplets (small ω) and low concentrations (low ϕ), the signal-to-noise ratio

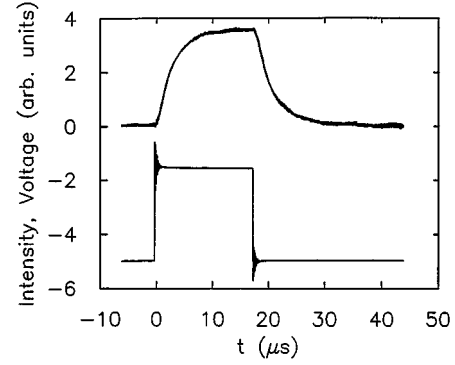


FIG. 2. Kerr electro-optical response. The upper curve is the Kerr electro-optical response from a sample with $\phi = 10\%$ and $\omega = 30$. The signal is digitized from the photodiode detector. The electric birefringence in this case is positive. For a sample with $\omega < 20$, a corresponding negative signal can be observed. For comparison, we also plot the applied E field as a function of time, which is shown by the lower curve.

is of more importance than the Joule heating. In this case, a large number of pulses was applied, and the transmitted light intensity was averaged using a digital oscilloscope (HP-54600A). For samples with large droplets (large ω) and high concentrations (large ϕ), the Joule heating is a severe problem, since fluid convection could be induced in the sample. Accompanying the convection, the sample turned cloudy, and the transmitted light intensity I_0 decreased with time. To minimize the heating effect, only a small number of pulses, with a long delay time, was applied to the sample. Fortunately, for microemulsions with large ϕ and ω , the optical signal is often so strong that even a couple of pulses are sufficient for an accurate determination of K .

The Kerr coefficient in this experiment was determined by steady-state measurements. The upper curve in Fig. 2 shows variations of the transmitted light intensity, $\Delta I (\equiv I - \alpha^2 I_0)$, which is proportional to the output voltage of the diode, as a function of time t . The measurement was carried out for a water-AOT-decane microemulsion with $\phi = 10\%$ and $\omega = 30$. As a reference, the E field as a function of time is also plotted as the lower curve in Fig. 2. The light intensity ΔI shows a transient relaxation when the field is applied, and eventually levels off. The steady-state value of ΔI is positive for this sample. If a similar measurement is carried out for a sample with $\omega < 20$, the steady-state value of ΔI will be negative, indicating a negative Kerr coefficient [14].

For each sample, measurements such as those shown in Fig. 2 were repeated for different E values. For all samples, ΔI was found to scale as E^2 , even for fields as large as 10^5 V/cm. The E^2 dependence suggests that the measurements are well within the linear (or Kerr) regime. From the slopes of the ΔI vs E^2 plots we derive the optical anisotropy Δn , which then gives the Kerr coefficient $K \equiv \Delta n / E^2$.

III. OBSERVATIONS

A. Effects of droplet size and concentration on the Kerr coefficients

Our first set of experiments consists of using a series of samples that have fixed concentrations ϕ , but with ω as an

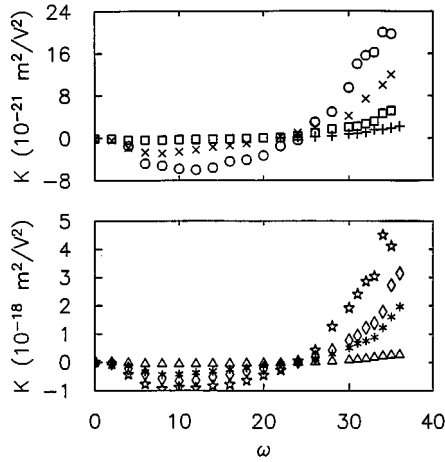


FIG. 3. Kerr coefficients K vs ω for different concentration ϕ . The upper figure is for the low concentration regime, covering $\phi=1\%$ (pluses), 1.5% (open squares), 3% (crosses), and 3.5% (open circles). The lower figure is for the high concentration regime, covering $\phi=7.5\%$ (open triangles), 20% (asterisks), 25% (open diamonds), and 30% (open stars). Despite more than two orders of magnitude change (see different vertical scales used in the upper and lower figures) in K as ϕ varies from 1% to 30% , the dependence of K on ω appears identical. That is, for a given ϕ , K decreases first, passes through a minimum at $\omega_{\min}\approx 9$, and then increases monotonically as ω increases.

independent variable. The concentrations were then varied systematically from 1% to 30% . To illustrate consistency between different sets of measurements (with different ϕ), all data are plotted together in Fig. 3. The upper figure (a) shows the low concentration regime ($\phi < 4\%$); whereas the lower figure (b) shows the high concentration regime ($\phi > 7\%$). Here a markedly strong ϕ dependence is observed, i.e., K changes by more than three orders of magnitude for the concentrations used in the experiment. A conspicuous feature of these measurements is that despite orders of magnitude change in K , the Kerr coefficient as a function of ω appears similar for all different ϕ . That is, a typical curve starts from $K=0$ at $\omega=0$, becomes progressively more negative as ω increases, and reaches a minimum at approximately $\omega_{\min}\approx 9$. After this point, K begins to increase, yielding zero at $\omega\approx 24$. By further increasing ω , K becomes a rapidly increasing function of ω . The behavior observed here is somewhat similar to electrorheological fluids, where both optical and mechanical properties of the fluids exhibit extreme sensitivity to small amounts of water present in the sample [15].

Upon close inspection of the data near the regime where K changes sign, we found that, while in the high concentration regime ($\phi > 7\%$) $\omega_C(\approx 24)$ is nearly a constant, independent of ϕ , the data show a subtle decrease in the low concentration regime. As shown in the inset of Fig. 4 (or Table II), the crossover ω_C changes by $\sim 10\%$ in the concentration range $1 < \phi < 5\%$. This behavior may not be entirely surprising in that water has a low, but finite, solubility in oil. The effect becomes more acute for the low concentrations, since the actual volume of the dispersed phase is now lower than anticipated. The phenomenon seen here appears to be consistent with our neutron scattering observation, in

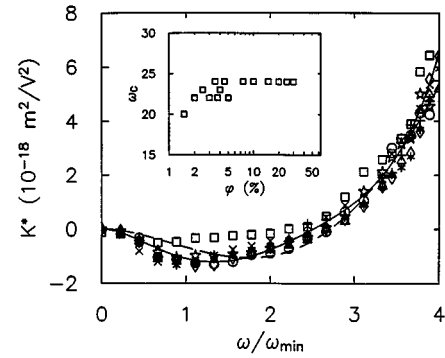


FIG. 4. Scaling plot. The data from Fig. 3 are plotted using $K^*=K(\phi=\text{const},\omega)/P(\phi)$, where P is a scaling factor which is a constant for a given ϕ . The horizontal axis ω is normalized by ω_{\min} , which is the minimum of the Kerr coefficients. Note that since the locations of the minimum do not vary appreciably with ϕ , ω_{\min} is set to a constant 9. Despite orders of magnitude change in K , the data at different ϕ can be collapsed quite satisfactorily, particularly at large ω . Some deviations were seen at the lowest concentration for $\omega/\omega_{\min} < 2$. The solid and dotted lines are polynomial fits; see text for more details. The inset is a plot of ω_C vs ϕ . For $\phi > 7\%$, $\omega_C(\approx 24)$ is independent of ϕ . However, at low concentrations ω_C decreases as ϕ decreases.

which we found that the microemulsion droplets become unstable upon dilution for ϕ below about a percent [5].

The similarity in the measured K vs ω curves for different ϕ suggests that there may be a scaling relationship between K and ϕ . For this reason we tried to superimpose all the data by dividing the measured Kerr coefficients at a fixed ϕ by a scaling factor $P(\phi)$, $K^*=K(\phi=\text{const},\omega)/P(\phi)$. Since all the data show a minimum at $\omega_{\min}\approx 9$, the horizontal axis is rescaled by ω_{\min} . The result of the above scaling procedures is shown in Fig. 4. As can be seen, the quality of the data collapsing is excellent, particularly for concentrations greater than 2% and for large ω . To see how K depends on ϕ we plot the scaling factor P as a function of ϕ on a log-log scale in Fig. 5. Here a linear relation is found indicating a power law of the form $P\sim\phi^\gamma$, where the γ turns out to be 2.3 ± 0.2 . The error bars shown in the figure are mainly due to uncertainties in bringing individual birefringence curves to collapse. It is surprising that the quadratic dependence appears to persist even at low concentrations, as shown in the inset of Fig. 5, where the data are plotted on a linear scale over the range $0\% < \phi < 5\%$. The solid line in the inset is a fit using $P=a\phi^2$, with a being the only adjustable parameter.

There has been much debate on whether or not K has a linear ϕ dependence at low concentrations [2,6–8]. Such a

TABLE II. The measured ω_C , ω_{\min} , and K_{\min} for different oils. All samples have $\phi=10\%$.

Name	ω_C	ω_{\min}	K_{\min} (m^2/V^2)
C_6H_{14} (hexane)	31 ± 2	8 ± 1	-2.2×10^{-21}
C_8H_{18} (octane)	29 ± 2	10 ± 1	-1.2×10^{-20}
C_9H_{20} (nonane)	27 ± 2	8 ± 1	-1.8×10^{-20}
$\text{C}_{10}\text{H}_{22}$ (decane)	24 ± 2	8 ± 1	-7.1×10^{-20}
$\text{C}_{12}\text{H}_{26}$ (dodecane)	20 ± 2	8 ± 1	-7.9×10^{-20}

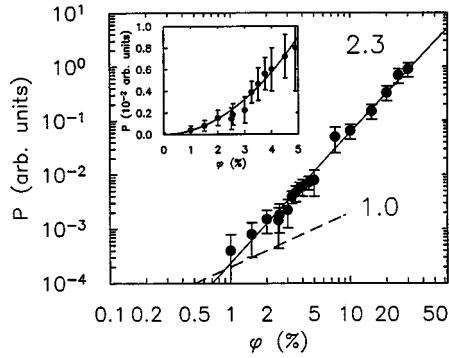


FIG. 5. The scaling factor P vs ϕ . P spans more than three decades and appears to be linear on the double logarithmic plot. A linear least square fit gives $P \sim \phi^\gamma$, with $\gamma = 2.3 \pm 0.2$. The inset is a linear plot for the low concentration data with the solid line calculated according to $P = a\phi^2$, where a is the free adjustable parameter. We note that in order for the single droplet model to be valid, γ should be unity at low concentrations, as shown by the dashed line, which is not obviously the case in this experiment. The fact that γ is close to 2 suggests that interactions between the droplets are significant.

linear dependence, if it exists, is significant, and may be used to determine bending elastic constants of microemulsion droplets [7,8]. In light of this we performed additional measurements using samples for which ω was fixed at a constant value, but ϕ was varied by dilution with decane. This method allows more systematic variations of ϕ , and was used by previous investigators to find the linear concentration dependence [7,8]. Figure 6(a) shows two sets of measurements with $\omega = 10$ and 32, which correspond to the negative and the positive Kerr responses, respectively. The solid and dashed lines are fits to a quadratic equation $K = a\phi^2$ without the linear term. Though a is the only adjustable parameter, reasonably good fits are achieved here. An alternative method to check the linear ϕ dependence is to divide the

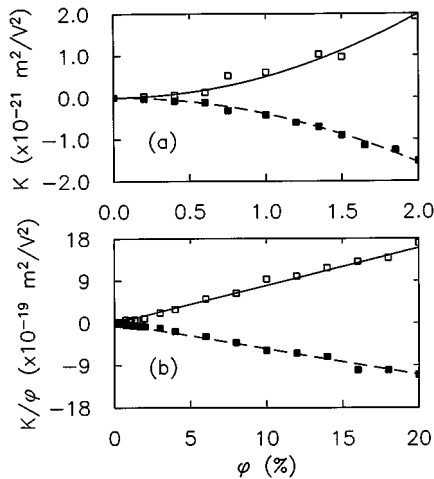


FIG. 6. Concentration dependence. The solid squares are for $\omega = 10$, and the open squares are for $\omega = 32$. In (a) the Kerr coefficient is plotted against ϕ for small concentrations. The solid and dashed lines are quadratic fits to the data. In (b) the ratio K/ϕ is plotted against ϕ . Note that both sets of data give nearly zero intercept, showing the absence of the linear ϕ dependence in K .

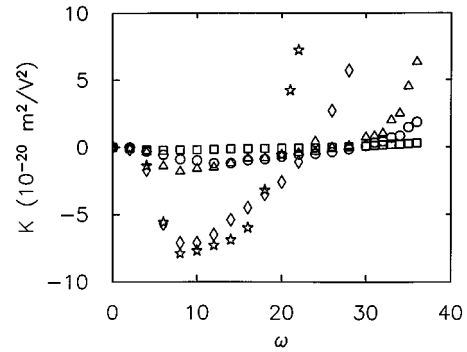


FIG. 7. Kerr coefficient K vs ω for different oils. The measurements are for five different oils: hexane (open squares), octane (open circles), nonane (open triangles), decane (open diamonds), and dodecane (open stars). For all the measurements, the droplet concentration is fixed, $\phi = 10\%$. As the hydrocarbon chain length increases, the Kerr effect becomes stronger, and the birefringence switches sign at smaller values of ω .

Kerr coefficient K by ϕ , and plot K/ϕ vs ϕ . The linear ϕ dependence in such a plot will be shown as a nonzero intercept. This is carried out in Fig. 6(b), and we found the intercept to be nearly indistinguishable from zero. The uncertainty in the measurements is about $\pm 5 \times 10^{-21} \text{ V}^2/\text{cm}^2$, which is a factor of 10–1000 smaller than those previously reported [7,8]. We speculate that the difference between the current measurements and those of earlier ones are likely due to the significantly improved sensitivity in our experiment. Our new measurements indicate that within our instrumental accuracy, the linear ϕ dependence of K cannot be reliably measured. The only feature that we observed, throughout the entire concentration range $0 < \phi < 30\%$, is the ϕ^2 dependence.

B. Effects of different aliphatic oils on the Kerr coefficients

In an attempt to explore the effects of different oils on the Kerr coefficients, alkanes of different chain lengths were used. The low-frequency ($\omega \rightarrow 0$) dielectric constant $\epsilon(0)$, which for oils is essentially the square of the optical index of refraction $\epsilon(0) \approx n^2$, increases monotonically as the molecular weight increases, as shown in Table I. The measurements were carried out for a set of samples all having $\phi = 10\%$ and ω as a variable. Figure 7 shows the experimental results. While the general trends are similar to that seen in the samples made of decane, a number of new features emerge. First, the locations of the minima in K do not change significantly for different oils, and these locations are approximately around $\omega_{\min} \approx 8$. Second, the magnitude of the negative part of the birefringence increases remarkably with increasing chain length. The minima K_{\min} change by nearly an order of magnitude for oils with short chains as compared to those with long chains. The tenfold change in K is quite significant, considering that either the low-frequency dielectric constant $\epsilon(0)$ or the refractive index n of the oils changes at most by about 10% as shown in Table I. Finally, it is noted that there is a systematic shift of ω_C toward smaller values as the oil chain length increases. The variation observed in the experiment is about 30% which is greater than that seen in dilute water-AOT-decane microemulsions,

as discussed above. The measured ω_{\min} , K_{\min} , and ω_C for different oils are listed in Table II.

IV. COMPARISON BETWEEN THEORY AND EXPERIMENT

A. Single droplet model

Within the single-droplet approximation, K can be calculated using the Clausius-Mossotti equation, taking into account the elastic deformation of the microemulsion droplets [7]. Though the detailed derivation is tedious, the qualitative result can be easily obtained by simple dimensional arguments. In the linear response regime, K is proportional to both the low- and high-frequency polarizabilities [$\alpha(0)$ and $\alpha(\varpi)$] of the fluid, where the low-frequency part couples to the applied external electric field while the high-frequency part couples to the probing electromagnetic waves, the laser light in this case. It is further assumed that both $\alpha(0)$ and $\alpha(\varpi)$ are linear combinations of two terms, one from the water core (α_w) and one from the surfactant layer on the water-oil interface (α_s), where α_i represents molecular polarizability of the corresponding component i . This gives

$$K \sim \left(\frac{4\pi}{3} R_w^3 \Delta \alpha_w(\varpi) + 4\pi d R_w^2 \Delta \alpha_s(\varpi) \right) \times \left(\frac{4\pi}{3} R_w^3 \alpha_w^*(0) + 4\pi d R_w^2 \alpha_s^*(0) \right) \rho,$$

where R_w is the water-core radius of the microemulsion droplets; d is the interfacial thickness, which is approximately the length of a surfactant molecule; $\Delta \alpha(\varpi)$ is the optical polarizability anisotropy; and $\alpha^*(0)$ is an effective low-frequency polarizability. Since $\rho \sim \phi/R_w^3$, the above equation predicts that: (1) K is linearly proportional to ϕ , at least at low concentrations, and (2) K is a polynomial of R_w with the lowest order term being proportional to R_w and the highest order term $\sim R_w^3$. For $R_w \gg d$, and assuming that all the surfactants stay on the interface, it can be seen that $R_w \sim \omega$, i.e., the volume-to-surface ratio of the droplet. In this case we expect that the leading term of the birefringence should scale as $K \sim \omega^3$ in the limit of large droplets.

Our experimental results deviate significantly from the above theoretical prediction. If the single-droplet model is correct, one would expect that the scaling factor P , shown in Fig. 5, would deviate from the ϕ^2 dependence at low concentrations. Here instead of seeing $P \sim \phi^2$, a linear dependence is expected. For this reason, $P \propto \phi$ is plotted in Fig. 5 using a dashed line. Clearly this scaling behavior is inconsistent with our observation. The most convincing evidence of the lack of linear ϕ scaling is seen in Fig. 6, as the samples in this plot were better controlled in their concentrations than those in Fig. 4. The single-droplet model cannot explain quantitatively the observed ω dependence either. Our data for K vs ω , as shown in Fig. 3, do not obey $K \sim \omega^3$ for large ω . To illustrate this, we show in Fig. 4 the polynomial fit to the data using the following functional form:

$$K^* = \sum_{m=2}^5 C_m (\omega/\omega_{\min})^m,$$

TABLE III. Coefficients of polynomial fits.

Order of polynomials	C_2	C_3	C_4	C_5
Fifth	-3.179	2.893	-0.899	0.100
Fourth	-1.196	0.566	-0.046	

where C_m are the fitting parameters and are listed in Table III. It is not difficult to see from our data that the zeroth and first order terms are negligible, as K^* exhibits a local maximum at the origin, $\omega/\omega_{\min}=0$. The entire curve in Fig. 4 can be adequately mimicked by the given function with four adjustable parameters delineated by the solid curve. To appreciate the importance of the fifth order term, the leading term for ω/ω_{\min} being large, we attempted to fit our data with only three parameters, C_2 , C_3 , and C_4 . This is shown by the dotted line in the figure. Here the quality of the fit is poor as indicated by the mismatch of the minimum in K^* and significant deviations at large ω/ω_{\min} . In fact, in this case C_4 turns out to be negative, as seen in Table III, which is against the trend observed in the measurements. The large deviations observed in both the ϕ and the ω dependences lead us to believe that the physical origin of the Kerr effect in our microemulsions is due to a collective effect of the microemulsion droplets rather than the shape deformation of individual droplets.

B. Dimer model

The simplest model that takes into account particle correlation is to assume droplets forming dimers. Mayer's model is based on this dimer structure of microemulsions [10]. Generally, the largest polarizability is along the direction of the dimer axis for both the static and optical electric fields. The Kerr effect would be positive if the dimer axis tends to be aligned along the field direction. However, if there exists a large permanent dipole moment μ , perpendicular to the dimer axis, the external field would rotate the permanent dipole toward the field direction. Under this condition, the dimer axis tends to be perpendicular to the field direction. This contribution to the Kerr effect is negative. In Mayer's model it was assumed that the permanent dipole moment is due to an electron charge partially trapped in the joint region between two adjacent droplets. The average polarizability anisotropy in the electric field is given by

$$\delta\alpha(\varpi) = \frac{2}{45} \beta E^2 [\Delta\alpha(0) - \beta\mu^2] \Delta\alpha(\varpi),$$

where $\Delta\alpha(0)$ and $\Delta\alpha(\varpi)$ are the low-frequency and optical polarizability anisotropy of the dimer in its intrinsic frame of reference, and $\beta = 1/k_B T$. If the dimer density ρ_d is proportional to the square of monomer density ρ_m , the ϕ^2 scaling behavior would be automatically built into Mayer's model.

In Mayer's model the number of dimers was not addressed, and the magnitude of the electric birefringence was treated as an overall factor to fit the experimental data. However, an estimate for ρ_d shows that the required number density ρ_d is too large. This is because the strength of the dimer-field interaction is weak in comparison to the thermal energy, and the alignment of dimers in the field direction is small.

The large Kerr coefficients found in our experiment require a large number of dimers. A simple calculation shows that ρ_d is at least of the same order of magnitude as ρ_m , and, for large concentrations, it is an order of magnitude larger than ρ_m . This means that even if the dimer structure dominates the birefringence, the number of dimers will reach a saturation, and ρ_m^2 dependence will break down. Therefore, Mayer's model is also inconsistent with the concentration dependence found in our experiment. This also implies that other theoretical models that stop at the dimer level are perhaps not sufficient to account for the large birefringence signal seen in the experiment.

Another experimental fact is that the crossover point ω_C is independent of ϕ when ϕ is sufficiently large. The prediction on the crossover point is also a crucial test for a successful model. For instance, a notable shift in ω_C was observed in our experiment when different oils were used. As shown in Table II, ω_C shifts from 31 for hexane to 20 for dodecane. Mayer's model predicts that the crossover point ω_C has nearly no dependence on the dielectric constant of the oil continuum due to the fact that $\epsilon(0)$ for water is much greater than that of oils.

V. CONCLUSION

In this paper we show that current theoretical models [7,10], which admittedly have played an important role in our understanding of the Kerr electro-optical effect in ternary microemulsions, are inadequate in giving a quantitative description of the AOT microemulsion. It is shown that the dimer model [10], which, though giving qualitatively correct features, as seen in our Kerr coefficient measurements, yields incorrect estimates for the number of dimers present in the

samples. We note that in recent years there have been systematic studies of the clustering phenomena in microemulsions. Such a phenomenon can be seen in electric conductivity, diffusion coefficients, and shear viscosity measurements [16]. In particular the binding energy for dimerization has been estimated using electric birefringence measurements similar to the present work [17]. However, Ref. [17] did not address the issue of the number of dimers nor checked if the numbers were consistent with the observed birefringence signal.

A conclusion which can be drawn from our observations is that many-body correlations, or particle clustering, must be responsible for the phenomenon observed. We conjecture that the presence of both positive and negative birefringence is a direct consequence of such a clustering effect. Similar to earlier theoretical models [7,10], two competing mechanisms must be operating, i.e., (i) the internal rearrangements of droplets in a cluster, and (ii) the overall shape change of the cluster in the presence of an \vec{E} field. Moreover, interfacial structures of surfactant monolayers and possibly the surrounding oil molecules, which couple to the rearrangements of the droplets, may also need to be taken into consideration.

ACKNOWLEDGMENTS

We have benefited from many helpful discussions with W. I. Goldberg, W. E. Henry, R. Kusner, K. Y. Min, and A. Onuki. We also acknowledge technical assistance from Y. H. Hwang, B. Martin, and C. Nebolisa. This work was supported by the NIH under Grant No. GM08206, the ACS under Grant No. PRF 30083-AC9, and by NASA under Grant No. NAS3-2789.

-
- [1] K. Y. Min, R. A. Wilkinson, G. Zimmerli, R. E. Kusner, and A. Onuki (unpublished).
- [2] M. E. Edwards, Y. H. Hwang, and X. L. Wu, *Phys. Rev. E* **49**, 4263 (1994).
- [3] L. D. Landau and E. M. Lifshitz, *Electrodynamics of Continuous Media* (Pergamon, Oxford, 1984), Chap. II, Sec. 11.
- [4] S. H. Chen, T. L. Lin, and J. S. Huang, in *Physics of Complex and Supermolecular Fluids*, edited by S. A. Safran and N. A. Clark (Wiley, New York, 1987), p. 285.
- [5] X. L. Wu, P. Tong, and J. S. Huang, *J. Colloid Interface Sci.* **148**, 104 (1992).
- [6] A. M. Cazabat, *Adv. Colloid Interface Sci.* **38**, 33 (1992).
- [7] E. Van der Linden, S. Geiger, and D. Bedeaux, *Physica A* **156**, 130 (1989); G. J. M. Koper, C. Roman Vas, and E. Van der Linden, *J. Phys. II* **4**, 163 (1994).
- [8] M. Borkovec and H. F. Eicke, *Chem. Phys. Lett.* **157**, 457 (1989).
- [9] M. Paillette and N. Belhadj-Tahar, *Prog. Colloid Polym. Sci.* **79**, 257 (1989).
- [10] G. Mayer, *Chem. Phys. Lett.* **168**, 575 (1990).
- [11] X. L. Wu, C. Yeung, M. W. Kim, J. S. Huang, and D. Ouyang, *Phys. Rev. Lett.* **68**, 1426 (1992).
- [12] E. Fredericq and C. Houssier, *Electric Dichroism and Electric Birefringence* (Clarendon, Oxford, 1973).
- [13] R. Piazza, V. Degiorgio, and T. Bellini, *Opt. Commun.* **58**, 400 (1986).
- [14] We note that the method of our measurement is quite different from that of Cazabat [6], who studied electric birefringence in a ternary water-in-benzene microemulsion. The negative birefringence was determined by a sharp negative spike immediately after the applied electric pulse. Since it is not entirely clear why the Kerr electro-optical response would have such a sharp down-turn, we cannot comment on the significance of the measurements.
- [15] A. P. Gast and C. F. Zukoski, *Adv. Colloid Interface Sci.* **30**, 153 (1989).
- [16] S. H. Chen, J. Rouch, F. Sciortino, and P. Tartaglia, *J. Phys. Condens. Matter* **6**, 10 855 (1994).
- [17] G. J. M. Koper, W. F. C. Sager, J. Smeets, and D. Bedeaux, *J. Phys. Chem.* **99**, 13 291 (1995).